

A Bayesian Adaptive Smoothing and Thresholding Approach for Activation Detection in Single-Subject fMRI

Juan Esteban Flórez Coronel

University of Puerto Rico, Mayaguez
Department of Mathematical Sciences



Advisor: Israel Almodóvar-Rivera, Ph.D.

June 25, 2024



Contents

1 Introduction

- What is fMRI?
- Previous Works

2 Objectives

3 Methods

4 Experiments

5 Experiments Results

6 BFAST in Real Data

7 Conclusions

- Future Work

8 References



What is fMRI?

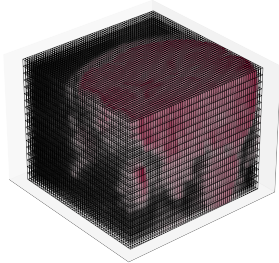


Figure 1: Voxels in fMRI Image

- Functional Magnetic Resonance Imaging (fMRI) is a non-invasive technique that takes a series of MRI captures in a certain period of time to analyze the behavior of the studied body part in the elapsed time, normally, the body part is stimulated to study its effect [1].
- In fMRI, the brain image is divided into 3D unit volumes called voxels, typically, more than 10^5 per image.



BOLD

- The most common technique to generate images is the Blood Oxygenation Level-Dependent (BOLD).
- BOLD measures the local changes in deoxyhemoglobin concentration in the brain.
- The change in oxygenation produces different local magnetic fields.



Hemodynamic Response Function

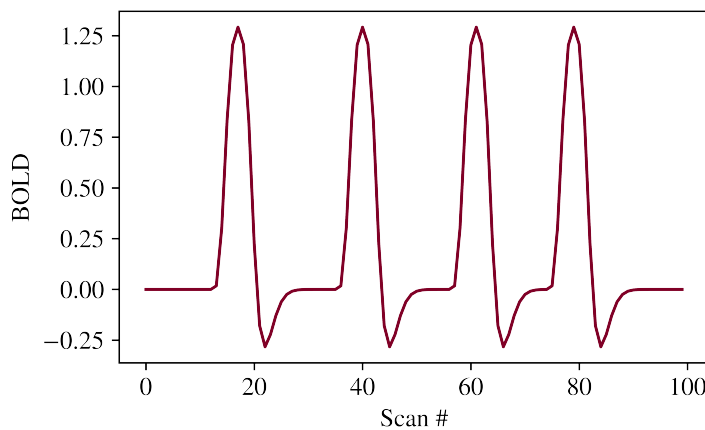


Figure 2: Glover Hemodynamic Response Function



Previous Works

- Identification of brain regions involved in language processing, memory, and decision-making [2, 3, 4].
- Identification of brain regions that are activated in response to specific stimuli or task [5, 6, 7].
- Methods used include time-series analysis, statistical parametric mapping, multivariate pattern classification, Bayesian modeling, among others [8, 9, 10, 11].
- Adaptive Smoothing and Thresholding (AST) method is also used by several researchers [12, 13, 14, 15].



Objectives

- Perform Bayesian time-series analysis to obtain a posterior probability map of an fMRI image for a single-subject situation.
- Develop an AST method that inputs the probability posterior map and finds the possible activated voxels.
- Study the proposed algorithm in different experimental setups in terms of similarity, rate of false positives, and activation percentage.
- Finally, apply the algorithm in a real fMRI experiment.



Time Series Model

- Let y_i be the response variable of the i th voxel, \mathbf{X} be the design matrix of the study containing the expected BOLD change and β_i be the coefficient that contains the stimulus, then:

$$\mathbf{y}_i \sim N(\mathbf{X}\beta_i, \Sigma)$$

- Note that Σ can have any structure, however, if we let $\Sigma = \sigma^2 \mathbf{I}$, the independent model is obtained:

$$\mathbf{y}_i | \beta_i, \sigma, \mathbf{X} \sim N(\mathbf{X}\beta_i, \sigma^2 \mathbf{I})$$



Bayesian Approach

- Using a noninformative prior distribution:

$$\pi(\beta_i, \sigma) \propto \frac{1}{\sigma^2}$$

- Using the Bayes' rule and the ordinary least squares solution to a linear problem $\hat{\beta}_i = (\mathbf{X}^T \mathbf{X})^{-1} \mathbf{X}^T \mathbf{y}_i$, the conditional posterior of β_i , given σ is then:

$$\pi(\beta_i | \sigma, \mathbf{X}, \mathbf{y}_i) \sim N\left(\hat{\beta}_i, (\mathbf{X}^T \mathbf{X})^{-1} \sigma^2\right).$$



Posterior Probability Maps

- For each voxel, i , in the region of interest, we calculate the posterior probability that the coefficient associated with the stimulus t has a positive effect in the BOLD response. This is roughly estimated using:

$$P(\beta_{i,t} > 0 | \mathbf{y}_i, \mathbf{X}).$$

- Let $\mathbb{P} = \{P(\beta_{i,t} > 0 | \mathbf{y}_i, \mathbf{X})\}_{i=[1,v]}$ represent a posterior probability map, where v is the number of voxels in the region of interest of an fMRI experiment.



Posterior Probability Map

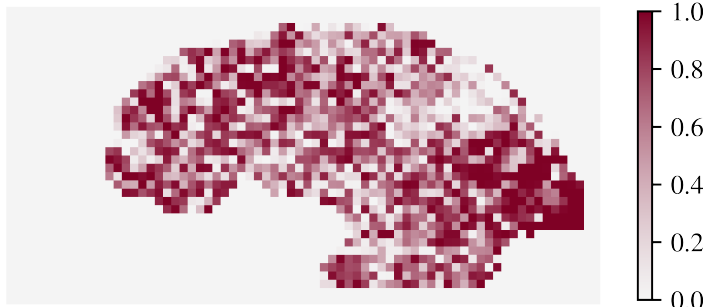


Figure 3: Axial View of a Posterior Probability Map



Relevant Distributions

- We will study \mathbb{P} as a Truncated Normal (TN) Distribution in the interval $[0, 1]$.
- $TN(0, 1)$ is in the domain of maximal attraction of the limiting distribution G , a Gumbel distribution.
 - Therefore, $TN^\nu(a_\nu x + b_\nu) \rightarrow G(x)$.
 - For $a_\nu = [\nu\psi(b_\nu)]^{-1}$ and $b_\nu = \Psi^{-1}(1 - 1/\nu)$.
 - Where ψ and Ψ are the PDF and CDF of the TN , respectively.



Gaussian Kernel Smoothing

- Convolution of the image with:

$$G(x, y) = \frac{1}{2\pi\sigma_s^2} \exp\left(-\frac{x^2 + y^2}{2\sigma_s^2}\right).$$

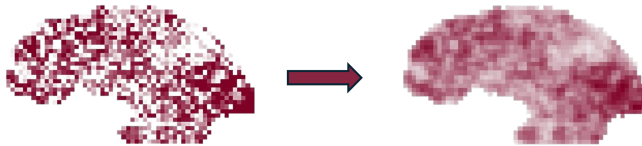


Figure 4: Example of the Smoothing Process in Posterior Probability Map
Using $\sigma_s = 100$

Jaccard Index (JI)

- Used to calculate image similarity: $J(A, B) = \frac{|A \cap B|}{|A \cup B|}$

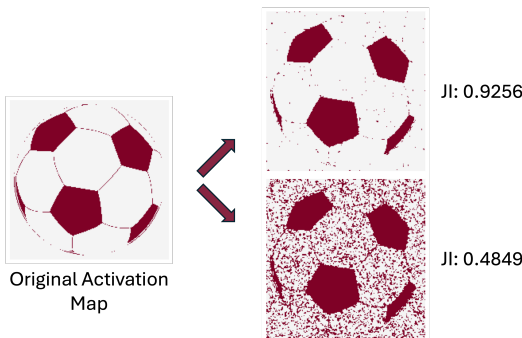


Figure 5: Example of Similarity Measurement Using JI

BFAST Algorithm

■ Initialization

- $\mathbb{P}^{(0)} = \mathbb{P}$
- $\zeta_i \equiv 0 \forall i$, where ζ_i is 1 when voxel i is activated and 0 if not.
- $\zeta_i^{(0)} \equiv \zeta_i$
- $v_0 = v$, where v_k is the number of voxels for which $\zeta_i^{(k)} = 0$.



BFAST Algorithm

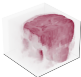
- For $k = 1, 2, \dots$, iterate as follows:
 - *Smoothing.* Smooth $\mathbb{P}^{(k-1)}$ using a Gaussian Kernel to obtain $\mathbb{P}^{(k)}$. Let $\sigma_s = 0.65 + 100(k - 1)$.
 - *Thresholding.* This consists of three steps:
 - Estimate $\mathbb{P}^{(k-1)}$ as a TN.
 - Calculate a_v and b_v .
 - Calculate the probability threshold, $\eta = a_v \nu_{0.01} + b_v$, with $\nu_{0.01}$ be the upper-tail 0.01-value of the standard Gumbel Distribution.
 - *Activation:* Set $\zeta_i^{(k)} = 1$ if $\zeta_i^{(k-1)} = 0$ and the value of the i th voxel of $\mathbb{P}^{(k)}$ is greater than η . Calculate $v_k = \sum_{i=1}^V \zeta_i^{(k)}$.



BFAST Algorithm

■ Termination

- Declare no activation and terminate if $\zeta^{(1)} \equiv 0$.
- If $J(\zeta^{(k)}, \zeta^{(k-1)}) \geq J(\zeta^{(k+1)}, \zeta^{(k)})$, the algorithm terminates and the final activation map is $\zeta^{(k)}$.
- The maximum number of iterations is default to $k = 10$.

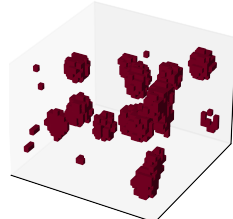
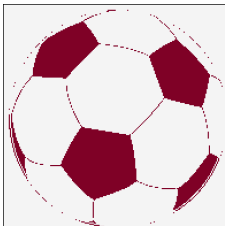


True Maps Summary

Table 1: Details of True Maps Considered. In both maps, dark voxels are active and light voxels are inactive.

Name	2D	3D
Dimensions	200×200	$40 \times 40 \times 25$
Voxels	40000	40000
A%	19.9375	3.9525

Map



3D Map Creation

- Step 1. Create a random 40×40 grid of numbers between 0 and 1. The ones that are greater than 0.99 take a value of 1, the rest are 0.
- Step 2. For each of those ones, select a random integer between 1 and 25 to be the depth of the cluster in the 3D grid.
- Step 3. At each of the cluster centers, generate a ball of radius 5. For each voxel inside that ball, randomly mark as active only the 67% of them.
- Step 4. Identify inactive voxels in each cluster that are surrounded by at least 4 active voxels. If so, mark it as active.



Design Matrix

- X will consist of 2 columns and one row per scan.
- The second column corresponds to the constant regressor.
- The first column contains the Glover Hemodynamic Response Function given the following event description:

Table 2: Event Description of Simulated fMRI Experiment

Parameter	Value
Number of Scans	100
Time Between Scans	2 seconds
Number of Stimulus	4
Duration of Each Stimulus	10 seconds
Time Between Stimulus	18 - 25 seconds



Design Matrix

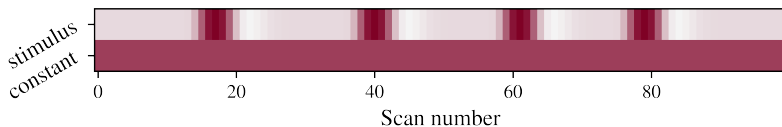


Figure 6: Transposed Design Matrix with Glover Hemodynamic Response and Constant Regressor



BOLD

- BOLD response without noise is computed depending on the voxel activation status, ζ_i , on the true map. See Table 3.

Table 3: Parameter Selection Based on Activation Status

Activation Status	Parameter Values
$\zeta_i = 0$	$\beta_i^* = (0, 100)^T$
$\zeta_i = 1$	$\beta_i^* = (75, 100)^T$

- BOLD response, \mathbf{y}_i , for each voxel i depends on the BOLD response without noise, $\mathbf{X}\beta_i^*$, and the noise generated using an ARMA Model, ϵ :

$$\mathbf{y}_i = \mathbf{X}\beta_i^* + \epsilon.$$



Noise with ARMA

- The noise (ϵ) is a vector of mean $\mu = 0$ and variance $\sigma^2 = 25^2$ with a baseline structure equivalent to:

$$ARMA_{\epsilon} (\{p_1, p_2, \dots\}, \{q_1, q_2, \dots\}).$$

- $p = |\{p_1, p_2, \dots\}|$ and $q = |\{q_1, q_2, \dots\}|$ are related to the order of the corresponding ARMA model, where p_a and q_b represent the coefficients of such models.
- $p, q \in [0, 1, 2, 3]$ were chosen to study the model under different noise scenarios. The values of p_a , and q_b were chosen arbitrarily as parameters. See Table 4.



Noise with ARMA

Table 4: Parameter Selection Related to ϵ

		p			
		0	1	2	3
		$\{ \}, \{ \}$	$\{\frac{1}{2}\}, \{ \}$	$\{\frac{1}{2}, \frac{3}{10}\}, \{ \}$	$\{\frac{1}{2}, \frac{3}{10}, \frac{1}{10}\}, \{ \}$
q	0	$\{ \}, \{\frac{1}{2}\}$	$\{\frac{1}{2}\}, \{\frac{1}{2}\}$	$\{\frac{1}{2}, \frac{3}{10}\}, \{\frac{1}{2}\}$	$\{\frac{1}{2}, \frac{3}{10}, \frac{1}{10}\}, \{\frac{1}{2}\}$
	1	$\{ \}, \{\frac{1}{2}, \frac{3}{10}\}$	$\{\frac{1}{2}\}, \{\frac{1}{2}, \frac{3}{10}\}$	$\{\frac{1}{2}, \frac{3}{10}\}, \{\frac{1}{2}, \frac{3}{10}\}$	$\{\frac{1}{2}, \frac{3}{10}, \frac{1}{10}\}, \{\frac{1}{2}, \frac{3}{10}\}$
2	0	$\{ \}, \{\frac{1}{2}, \frac{3}{10}, \frac{1}{10}\}$	$\{\frac{1}{2}\}, \{\frac{1}{2}, \frac{3}{10}, \frac{1}{10}\}$	$\{\frac{1}{2}, \frac{3}{10}\}, \{\frac{1}{2}, \frac{3}{10}, \frac{1}{10}\}$	$\{\frac{1}{2}, \frac{3}{10}, \frac{1}{10}\}, \{\frac{1}{2}, \frac{3}{10}, \frac{1}{10}\}$
	3	$\{ \}, \{\frac{1}{2}, \frac{3}{10}, \frac{1}{10}\}$	$\{\frac{1}{2}\}, \{\frac{1}{2}, \frac{3}{10}, \frac{1}{10}\}$	$\{\frac{1}{2}, \frac{3}{10}\}, \{\frac{1}{2}, \frac{3}{10}, \frac{1}{10}\}$	$\{\frac{1}{2}, \frac{3}{10}, \frac{1}{10}\}, \{\frac{1}{2}, \frac{3}{10}, \frac{1}{10}\}$



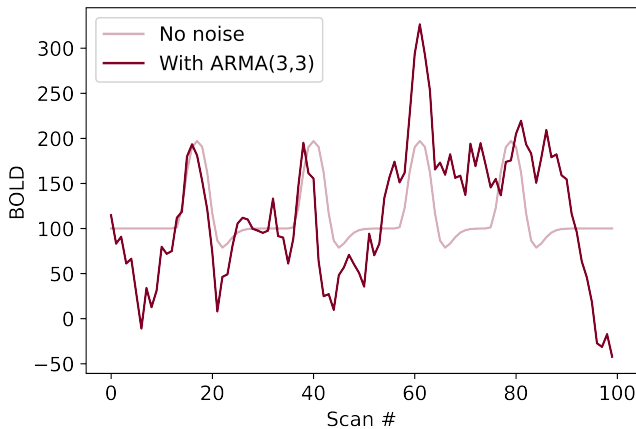


Figure 7: Example of BOLD Signal in Active Voxels With and Without Noise



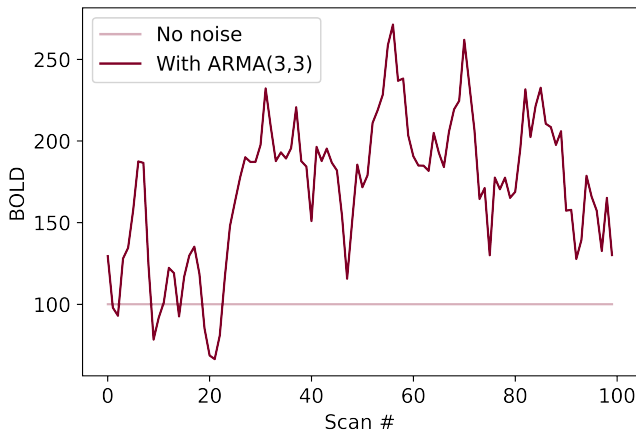


Figure 8: Example of BOLD Signal in Inactive Voxels With and Without Noise



SNR and CNR

- Signal-to-Noise Ratio (SNR) represents how strong the signal is with respect to the noise.
- Contrast-to-Noise Ratio (CNR) represents how significant is the BOLD change in activation regions with respect to the noise.



Noise in Simulations

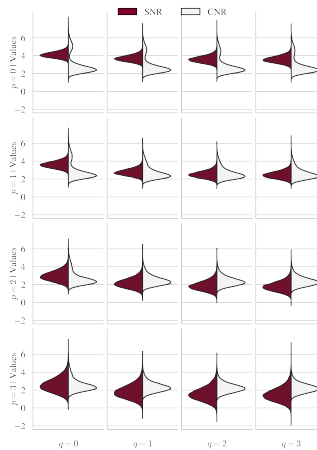


Figure 9: Numerical Distribution of the Voxel-Wise SNR and CNR Values of 2D Map

Noise in Simulations

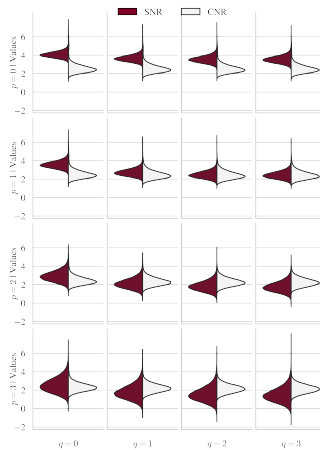


Figure 10: Numerical Distribution of the Voxel-Wise SNR and CNR Values of 3D Map

Noise in Simulations

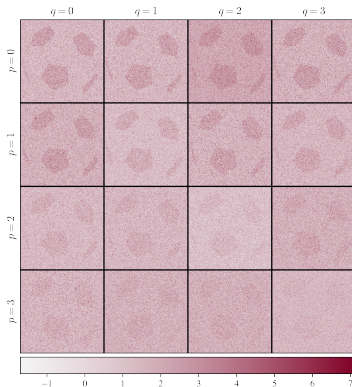


Figure 11: Spatial Distribution of the SNR Values in 2D Map

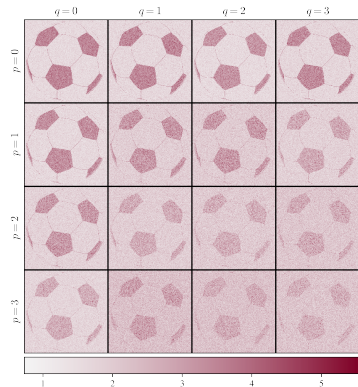


Figure 12: Spatial Distribution of the CNR Values in 2D Map



Example of BFAST Iterations

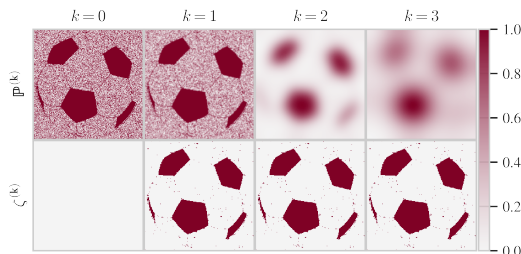


Figure 13: Example in 2D Map for $p, q = 0$

Example of BFAST Iterations

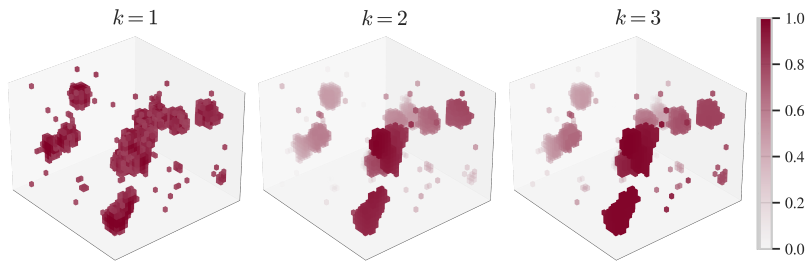


Figure 14: Example of 3D Maps for $p, q = 0$

Performance Metrics

- Performance of the BFAST algorithm was evaluated by comparing the final activation map with the true activation map using:
 - JI: Similarity between the two maps.
 - FPR: Ratio of the voxels marked as activated that are not really active and the total number of inactive voxels.
 - A%: Percentage of active voxels between both maps.

Performance Metrics

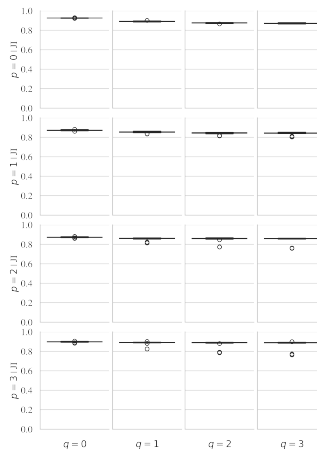


Figure 15: Jaccard Index in 2D Map

Performance Metrics

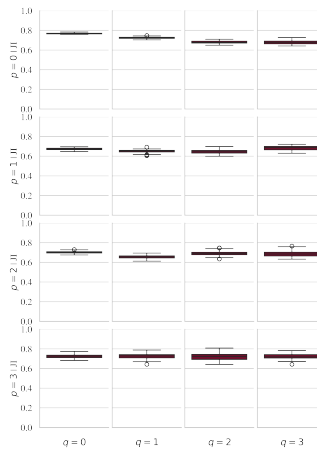


Figure 16: Jaccard Index in 3D Map

Performance Metrics

Table 5: Performance Metrics Summary in 2D Case

p	q	SNR	CNR	JI	FPR	A%
0	0	4.0841	3.0344	0.9256	0.0078	19.663
	1	3.6815	2.9342	0.8925	0.0180	20.515
	2	3.5788	2.9035	0.8754	0.0227	20.858
	3	3.5688	2.8960	0.8695	0.0244	20.995
1	0	3.5988	2.9042	0.8794	0.0222	20.870
	1	2.7538	2.6993	0.8509	0.0299	21.398
	2	2.5159	2.6191	0.8488	0.0308	21.475
	3	2.4691	2.6007	0.8533	0.0292	21.350
2	0	2.9564	2.7050	0.8685	0.0240	20.908
	1	2.1686	2.4761	0.8648	0.0267	21.228
	2	1.8753	2.3861	0.8578	0.0284	21.333
	3	1.8050	2.3646	0.8581	0.0283	21.313
3	0	2.5794	2.5607	0.8932	0.0174	20.445
	1	1.8416	2.3420	0.8882	0.0185	20.513
	2	1.5895	2.2576	0.8837	0.0200	20.638
	3	1.5260	2.2323	0.8793	0.0213	20.740



Performance Metrics

Table 6: Performance Metrics Summary in 3D Case

p	q	SNR	CNR	JI	FPR	A%
0	0	4.0430	2.6156	0.7677	0.0046	3.8075
	1	3.6401	2.5873	0.7249	0.0068	3.9950
	2	3.5348	2.5699	0.6796	0.0086	4.0675
	3	3.5233	2.5660	0.6767	0.0082	3.9950
1	0	3.5553	2.5687	0.6741	0.0092	4.1500
	1	2.7134	2.4836	0.6468	0.0108	4.2650
	2	2.4711	2.4406	0.6410	0.0116	4.3550
	3	2.4303	2.4320	0.6757	0.0099	4.2625
2	0	2.9143	2.4583	0.6979	0.0083	4.1125
	1	2.1205	2.3332	0.6566	0.0108	4.3100
	2	1.8440	2.2791	0.6909	0.0079	4.0075
	3	1.7735	2.2584	0.6859	0.0081	4.0300
3	0	2.5407	2.3554	0.7297	0.0065	3.9650
	1	1.8073	2.2290	0.7194	0.0067	3.9525
	2	1.5582	2.1729	0.7167	0.0074	4.0600
	3	1.5004	2.1515	0.7092	0.0066	3.8925

Real Life Application - Theory of Mind

- Theory of Mind fMRI experiment by Moran (2012) [16].
- 48 participants, most of them in their 20's and some other in their 70's.
- Gradient-echo echo-planar pulse sequence on a 3T Tim Trio MRI scanner



Data Description

- Stimulus are false belief question (fbq), false belief story (fbs), false photo question (fpq), and false photo story (fps).
- Data has dimensions $72 \times 72 \times 36$ of 2 mm isotropic voxels.
- 40078 Voxels in the Region of Interest
- BFAST identified 1766 active voxels (4.41 A%) on the false belief question stimulus in the try 1 of subject 1.



Design Matrix

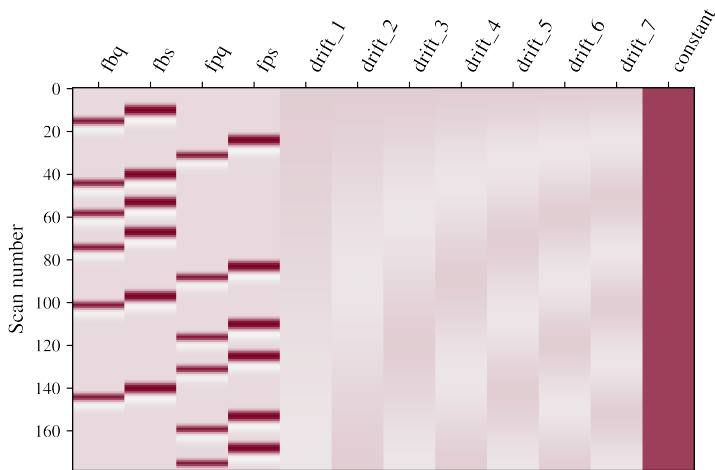


Figure 17: Design Matrix of the Experiment

BFAST Results

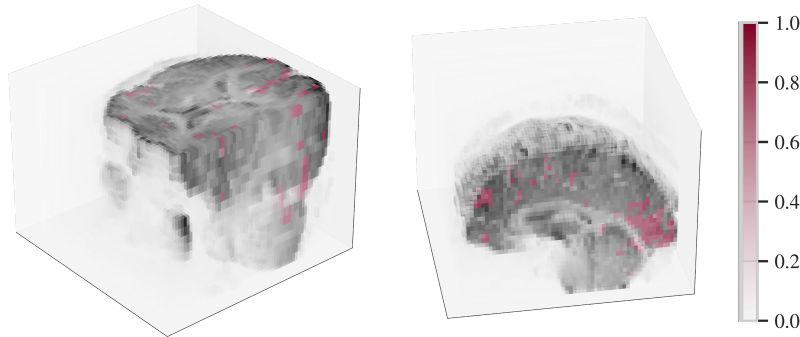


Figure 18: Activation Regions Identified by BFAST

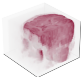
Conclusions

- BFAST algorithm in simulated frameworks:
 - 1600 scenarios of different dimension and noise.
 - With respect to the expected outputs:
 - Average similarity of 0.85.
 - False positive ratio below 0.02.
- BFAST algorithm in the theory of mind cognitive experiment:
 - Activation percentage of 4.41% is usual in fMRI.
 - Apparent activations in:
 - Prefrontal cortex because cognitive work stimulates memory.
 - Occipital lobe because the stimulus were presented visually.



Future Work

- Modify parameters from the BFAST algorithm such as the normalization coefficients, the computation of the threshold, and the smoothing coefficient, among others.
- Use the BFAST algorithm in other real life applications.



References I

- ❑ B. R. Buchbinder, "Functional magnetic resonance imaging," *Handbook of clinical neurology*, vol. 135, pp. 61–92, 2016.
- ❑ W. D. Gaillard, B. C. Sachs, J. R. Whitnah, Z. Ahmad, L. M. Balsamo, J. R. Petrella, S. H. Braniecki, C. M. McKinney, K. Hunter, B. Xu, *et al.*, "Developmental aspects of language processing: fmri of verbal fluency in children and adults," *Human brain mapping*, vol. 18, no. 3, pp. 176–185, 2003.
- ❑ A. Golby, G. Silverberg, E. Race, S. Gabrieli, J. O'Shea, K. Knierim, G. Stebbins, and J. Gabrieli, "Memory encoding in alzheimer's disease: an fmri study of explicit and implicit memory," *Brain*, vol. 128, no. 4, pp. 773–787, 2005.



References II

- DOC H. R. Heekeren, I. Wartenburger, H. Schmidt, H.-P. Schwintowski, and A. Villringer, "An fmri study of simple ethical decision-making," *Neuroreport*, vol. 14, no. 9, pp. 1215–1219, 2003.
- DOC J. Orchard, C. Greif, G. H. Golub, B. Bjornson, and M. S. Atkins, "Simultaneous registration and activation detection for fmri," *IEEE transactions on medical imaging*, vol. 22, no. 11, pp. 1427–1435, 2003.
- DOC T. Deneux and O. Faugeras, "Using nonlinear models in fmri data analysis: model selection and activation detection," *NeuroImage*, vol. 32, no. 4, pp. 1669–1689, 2006.

References III

-  B. A. Ardekani, J. Kershaw, K. Kashikura, and I. Kanno, "Activation detection in functional mri using subspace modeling and maximum likelihood estimation," *IEEE Transactions on Medical Imaging*, vol. 18, no. 2, pp. 101–114, 1999.
-  D. W. Adrian, R. Maitra, and D. B. Rowe, "Complex-valued time series modeling for improved activation detection in fmri studies," *The annals of applied statistics*, vol. 12, no. 3, p. 1451, 2018.
-  J. Marchini and A. Presanis, "Comparing methods of analyzing fmri statistical parametric maps," *Neuroimage*, vol. 22, no. 3, pp. 1203–1213, 2004.



References IV

-  J. A. Mumford, B. O. Turner, F. G. Ashby, and R. A. Poldrack, "Deconvolving bold activation in event-related designs for multivoxel pattern classification analyses," *Neuroimage*, vol. 59, no. 3, pp. 2636–2643, 2012.
-  S. Makni, J. Idier, T. Vincent, B. Thirion, G. Dehaene-Lambertz, and P. Ciuciu, "A fully bayesian approach to the parcel-based detection-estimation of brain activity in fmri," *Neuroimage*, vol. 41, no. 3, pp. 941–969, 2008.
-  K. Tabelow, J. Polzehl, H. U. Voss, and V. Spokoiny, "Analyzing fmri experiments with structural adaptive smoothing procedures," *NeuroImage*, vol. 33, no. 1, pp. 55–62, 2006.



References V

- 📄 M. A. Lindquist, J. M. Loh, and Y. R. Yue, “Adaptive spatial smoothing of fmri images,” *Statistics and its Interface*, vol. 3, no. 1, pp. 3–13, 2010.
- 📄 F. Strappini, E. Gilboa, S. Pitzalis, K. Kay, M. McAvoy, A. Nehorai, and A. Z. Snyder, “Adaptive smoothing based on gaussian processes regression increases the sensitivity and specificity of fmri data,” *Human brain mapping*, vol. 38, no. 3, pp. 1438–1459, 2017.
- 📄 I. Almodóvar-Rivera and R. Maitra, “Fast adaptive smoothing and thresholding for improved activation detection in low-signal fmri,” *IEEE Transactions on Medical Imaging*, vol. 38, no. 12, pp. 2821–2828, 2019.



References VI

-  J. M. Moran, E. Jolly, and J. P. Mitchell, "Social-cognitive deficits in normal aging," *Journal of neuroscience*, vol. 32, no. 16, pp. 5553–5561, 2012.

A% activation percentage. 7, 18, 33, 36, 37, 39

AST Adaptive Smoothing and Thresholding. 6, 7

BFAST Bayesian Fast Adaptive Smoothing and Thresholding.
15–17, 31–33, 39, 41–43

BOLD Blood Oxygenation Level-Dependent. 4, 8, 10, 22, 27

CNR Contrast-to-Noise Ratio. 27–30

fMRI Functional Magnetic Resonance Imaging. 3, 7, 10,
20, 38, 42

FPR False Positive Rate. 33, 36, 37

JI Jaccard Index. 14, 33–37

SNR Signal-to-Noise Ratio. 27–30

TN Truncated Normal. 12, 16

